Polymer adsorption on curved surfaces

Handan Arkin[1,2,*] and Wolfhard Janke[1,†]
[1]*Institut für Theoretische Physik, Universität Leipzig, Postfach 100 920, 04009 Leipzig, Germany*
[2]*Department of Physics Engineering, Faculty of Engineering, Ankara University, Tandogan, 06100 Ankara, Turkey*
(Received 14 September 2017; published 26 December 2017)

The conformational behavior of a coarse-grained finite polymer chain near an attractive spherical surface was investigated by means of multicanonical Monte Carlo computer simulations. In a detailed analysis of canonical equilibrium data over a wide range of sphere radius and temperature, we have constructed entire phase diagrams both for nongrafted and end-grafted polymers. For the identification of the conformational phases, we have calculated several energetic and structural observables such as gyration tensor based shape parameters and their fluctuations by canonical statistical analysis. Despite the simplicity of our model, it qualitatively represents in the considered parameter range real systems that are studied in experiments. The work discussed here could have experimental implications from protein-ligand interactions to designing nanosmart materials.

DOI: 10.1103/PhysRevE.96.062504

I. INTRODUCTION

The interaction of macromolecules with differently shaped substrates is particularly important for interdisciplinary research and nanotechnological applications including, e.g., the fabrication of biosensors [1] and peptide adhesion [2] to metals [3,4] or semiconductors [5–7]. Gaining knowledge of structure formation for a variety of interfaces has therefore been a challenging subject of numerous experimental, theoretical, and computational investigations. This includes thermodynamic studies of polymers at planar surfaces [8–26], and also under pulling force [27,28], and at curved surfaces such as nanotubes, nanostrings, and nanoparticles [29–34]. Polymer adsorption on substrates plays an important role within a wide perspective. Due to the many possible applications, these "hard-soft" hybrid systems have been extensively studied from all aspects. For instance, employing a single-chain mean-field theory for polymers grafted to a flat surface has featured different morphologies for which, by controlling the self-assembly conditions, nonaggregated chains can coexist with micelles [35]. Also in the context of self-consistent mean-field theory, finite chain-length (N) effects on the elastic properties of the substrate have been investigated by Skau and Blokhuis [36] to leading order in $1/N$ for both flat and curved geometries. The understanding of the conformational properties of a polymer requires systematic studies because of the cooperative effect of the monomers in response to different system conditions. The structuring effect of an attractive substrate results in a rich phase behavior caused by the competition between monomer-monomer and monomer-surface interaction.

By performing Monte Carlo simulations for detailed atomistic and generic coarse-grained lattice and continuum models, many studies have been done to investigate nanoparticle-polymer interactions for different geometries, such as cylinder and sphere [37]. Using computer simulations, Barr and Panagiotopoulos [38] studied a system of polymers grafted to a spherical nanoparticle in salt solution to gain insight into the conformational behavior of polymers on curved surfaces. Silver and gold nanoparticles have also been considered experimentally as a catalyst for enhanced amyloid peptide fibrillation [39–41]. In a recent study, the adsorption of a semiflexible polymer on flat and curved surfaces has been considered by Kampmann *et al.* [42] in the wormlike chain formulation, neglecting excluded-volume effects and monomer-monomer interactions. This is a good approximation in the limit of sufficiently stiff polymers with typically weakly bent conformations, allowing one to control the interplay of polymer stiffness, adsorption potential range, and curvature radius analytically. Taking in addition excluded-volume effects and monomer-monomer interactions into account, recent computer simulations for a semiflexible polymer showed a much richer phase structure already for a flat substrate, strongly depending on the polymer stiffness [26].

Tanaka *et al.* [43,44] examined the freezing transition of compact polyampholytes, for both single and multiple chains. There have been a number of studies of these systems to determine the effects of surface charge densities [45] and solvent conditions on the morphologies of polymer chains. Furthermore, adsorption of charged chains such as polyelectrolytes by oppositely charged surfaces is also an important aspect in surface and colloidal science [46,47]. Because of the electrostatic attraction between chains and surfaces, a charged chain tends to be adsorbed onto the surface. These studies are also extended to oppositely charged blocks on the chains [48], and Dobrynin and Rubinstein [49,50] addressed typical adsorption regimes for a salt-free environment using scaling-law arguments. The interaction between polyelectrolytes and small spheres of opposite charge is of interest for many problems such as interaction between polyelectrolytes and micelles or formation of the nucleosomal complex between DNA and proteins [51,52].

Given the plethora of specific applications, it is important to complement such detailed studies with investigations of generic models that focus on the most characteristic parameters of the systems and can hence provide a broad overview of the involved phenomena. In this spirit we have recently investigated the purely steric confinement effect of a spherical cage on a coarse-grained flexible polymer chain to determine the influence on the location of the collapse and freezing

*handan.olgar@eng.ankara.edu.tr
†wolfhard.janke@itp.uni-leipzig.de; http://www.physik.uni-leipzig.de/CQT.html

transitions [53]. Another hybrid system under consideration was a polymer chain *inside* an attractive spherical cage for which we have constructed the phase diagram depending on the attraction strength of the sphere inner wall and the temperature [54,55] and investigated the ground-state properties [56]. We have also compared the results with the case of an attractive flat surface [57]. Both systems exhibit a rich phase behavior ranging from highly ordered, compact to extended, random coil structures.

Here, we consider the opposite situation: A nanosphere whose attractive *outer* spherical surface is the target for the adsorbing polymer. This problem could have practical implications for a broad variety of applications ranging from protein-ligand binding, designing smart sensors to molecular pattern recognition [58–61] and for the discovery of new drugs that bind to specific receptors. Therefore it is interesting to study the adsorption of macromolecules on different types of substrates and identify the conformational changes that a polymer can experience at the interface. In this paper, we are going to investigate a simple coarse-grained polymer model interacting with a spherical surface of varying curvature by means of multicanonical Monte Carlo computer simulations. This method enables us to give an overview of the different structural phases of a flexible polymer chain over a wide range of sphere radius and temperature. In a comparative study, we consider the two cases of nongrafted and end-grafted polymer chains.

The rest of the paper is organized as follows. In Sec. II the model system is described in detail. Our model is a simple model that enables changing parameters on a broad scale, which allows mapping to different real systems that are considered in experiments. The primary parameters that are scanned to obtain two-dimensional phase diagrams are the radius of the nanoparticles and the temperature. We kept the adsorption strength constant in this study (whereas we varied it in another earlier study). Then, in Sec. III the multicanonical Monte Carlo simulation method is briefly reviewed and the measured observables are introduced, where special attention is paid to invariants of the gyration tensor. Section IV presents and discusses our main results, the phase diagrams for the two systems under consideration. Finally, Sec. V concludes the paper with a summary of our findings.

II. MODEL

A. Bead-stick polymer model

The polymer chain is described by a generic, coarse-grained continuum model for homopolymers which has also been used for studies of heteropolymers in the frame of the hydrophobic-polar model [62,63]. As in lattice models, the adjacent monomers are connected by rigid covalent bonds. Thus, the distance is kept fixed and set to unity, fixing the length scale. The contact interaction of lattice models is replaced by a distance-dependent $12-6$ Lennard-Jones (LJ) potential,

$$E_{\mathrm{LJ}} = 4\epsilon_{\mathrm{LJ}} \sum_{i=1}^{N-2} \sum_{j=i+2}^{N} \left[\left(\frac{\sigma}{r_{ij}} \right)^{12} - \left(\frac{\sigma}{r_{ij}} \right)^{6} \right], \qquad (1)$$

accounting for short-range excluded volume repulsion and long-range interaction of nonbonded monomers at distance $r_{ij} = |\vec{r}_i - \vec{r}_j|$. Each summand in (1) is minimized for $r_{ij} = 2^{1/6}\sigma$ where it contributes $-\epsilon_{\mathrm{LJ}}$ to E_{LJ}. In the simulations we set ϵ_{LJ} to unity, fixing the energy scale, and choose $\sigma = 1$. This model was first employed in two dimensions [62,63] and later generalized to three-dimensional AB proteins [64–66], partially with modifications taking implicitly into account additional torsional energy contributions of each bond. For consistency with our previous work [15,20,21,54–57,66] we kept a very weak bending energy $E_{\mathrm{bend}} = \varkappa \sum_{i=1}^{N-2} (1 - \cos\vartheta_i)$ with $\varkappa = 1/4$ and ϑ_i denoting the angle between adjacent bonds $[\cos\vartheta_i = (\vec{r}_{i+1} - \vec{r}_i) \cdot (\vec{r}_{i+2} - \vec{r}_{i+1})]$. For such a small bending stiffness, however, the statistical properties are hardly distinguishable from a truly flexible ($\varkappa = 0$) polymer (see, e.g., Fig. 1 in Ref. [67]).

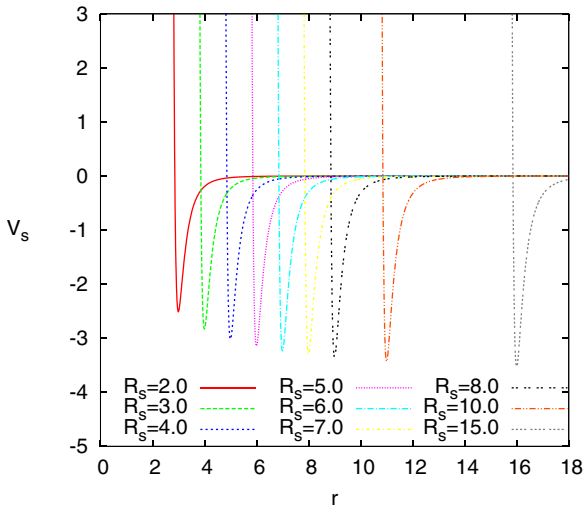

FIG. 1. The functional dependence of the attractive sphere potential (2) (with $\epsilon_{\mathrm{s}} = \sigma_{\mathrm{s}} = \epsilon = 1$) for different values of the sphere radius R_{s}.

B. Surface interaction

In this work, we assume that the polymer chain interacts with an attractive spherical surface. As in our previous work [54–57] the interaction of the polymer chain monomers and the attractive sphere is modeled by the surface energy $E_{\mathrm{s}} = \sum_{i=1}^{N} V_{\mathrm{s}}(r_i)$ where

$$V_{\mathrm{s}}(r_i) = 4\pi\epsilon_{\mathrm{s}} \frac{R_{\mathrm{s}}}{r_i} \left\{ \frac{1}{5} \left[\left(\frac{\sigma_{\mathrm{s}}}{r_i - R_{\mathrm{s}}} \right)^{10} - \left(\frac{\sigma_{\mathrm{s}}}{r_i + R_{\mathrm{s}}} \right)^{10} \right] - \frac{\epsilon}{2} \left[\left(\frac{\sigma_{\mathrm{s}}}{r_i - R_{\mathrm{s}}} \right)^{4} - \left(\frac{\sigma_{\mathrm{s}}}{r_i + R_{\mathrm{s}}} \right)^{4} \right] \right\}. \qquad (2)$$

Here R_{s} is the radius of the sphere, $r_i = (x_i^2 + y_i^2 + z_i^2)^{1/2} \geqslant R_{\mathrm{s}}$ is the distance of a monomer to the origin and x_i, y_i, z_i are the coordinates of monomers, and σ_{s}, ϵ_{s}, and ϵ are set to unity. The functional dependence of the potential $V_{\mathrm{s}}(r_i)$ is shown in Fig. 1 for selected R_{s} values which are used in the simulations. For sufficiently large spheres and r_i close to the surface, $r_i \approx R_{\mathrm{s}}$, we can neglect the terms $(\sigma_{\mathrm{s}}/2R_{\mathrm{s}})^{10}$ and

$(\sigma_s/2R_s)^4$ and approximate [57]

$$V_s(r_i) \approx 4\pi\epsilon_s\left[\frac{1}{5}\left(\frac{\sigma_s}{r_i - R_s}\right)^{10} - \frac{\epsilon}{2}\left(\frac{\sigma_s}{r_i - R_s}\right)^{4}\right], \quad (3)$$

which is a standard $10-4$ Lennard-Jones potential with $V_s^{\min} = -4\pi\epsilon_s(3/10)\epsilon^{5/3}R_s/(R_s + \sigma_s\epsilon^{-1/6})$ at $r_i^{\min} = R_s + \sigma_s\epsilon^{-1/6}$.

The total energy $E = E_{LJ} + E_{bend} + E_s$ governs the statistical properties at temperature T respectively thermal energy k_BT, where k_B is the Boltzmann constant. In the following we set k_B to unity, fixing the temperature scale. The most interesting phenomena result from the competition of intrinsic monomer-monomer and monomer-surface wall interactions. For instance in the case of adsorption of polyelectrolyte chains onto oppositely charged interfaces, the electrostatic potential controls the competition of polymer-surface adsorption-desorption behavior.

Our primary goal of this study is to obtain a broad overview of the phase diagram in the R_s-T plane. To make contact to specific experimental polymer-substrate systems one may identify the empirical (dimensionful) coupling parameters of, say, the Martini force field [68] with the (dimensionless) parameters of our coarse-grained model. For instance, from Table 1 in Ref. [69] we read off that methylene has $\epsilon_{phys} = 104 \times 8.31/1000 = 0.86$ KJ/mol which approximately corresponds to $\epsilon_{LJ} = 1.0$ in our model. It follows that the 20mer (four methylenes per bead) considered in our study corresponds approximately to n-C80. Similarly, the substrate maps approximately onto a polystyrene colloidal sphere, but its adsorption propensity is weaker than that of carbon or silica.

III. SIMULATION SETUP

A. Multicanonical method

In order to obtain statistical results of sufficient accuracy we applied the multicanonical (muca) Monte Carlo algorithm [70–72] (for reviews, see Refs. [73–75]), where the energy distribution is flattened artificially allowing, in principle, for a random walk of successive states in energy space. This flattening is controllable and therefore reproducible. To this end, the Boltzmann probability is multiplied by a weight factor $W(E)$, which in our case is a function of the total energy $E = E_{LJ} + E_{bend} + E_s$. Then the multicanonical probability for a state or conformation $\{\mathbf{x}\}$ with energy $E(\{\mathbf{x}\})$ reads $p_{muca}(E) = \exp(-E/k_BT)W(E)$, up to an unimportant multiplicative factor. In order to obtain a multicanonical or "flat" distribution, the initially unknown weight function $W(E)$ has to be determined iteratively: In the beginning, the weights $W^{(0)}(E)$ are set to unity for all energies letting the first run be a usual Metropolis simulation which yields an estimate $H^{(0)}(E)$ for the canonical distribution. This histogram is used to determine the next guess for the weights; the simplest update is to calculate $W^{(1)}(E) = W^{(0)}(E)/H^{(0)}(E)$. Then the next run is performed with probabilities $p^{(1)}_{muca}(E) = \exp(-E/k_BT)W^{(1)}(E)$ of states with energy E, yielding $H^{(1)}(E)$ and $W^{(2)}(E) = W^{(1)}(E)/H^{(1)}(E)$, and so on. The iterative procedure is continued until the weights are appropriate in a way that the multicanonical histogram $H(E)$ is "flat." After having determined accurate weights $W(E)$, they are kept fixed and following some thermalization sweeps a long production run is performed, where statistical quantities O are obtained multicanonically, $\langle O\rangle_{muca} = \sum_{\{\mathbf{x}\}} p_{muca}(E(\{\mathbf{x}\}))O(\{\mathbf{x}\})/Z_{muca}$ with the multicanonical partition function $Z_{muca} = \sum_{\{\mathbf{x}\}} p_{muca}(E(\{\mathbf{x}\}))$. The canonical statistics is obtained by reweighting the multicanonical to the canonical distribution, i.e., canonical expectation values are computed as $\langle O\rangle = \langle OW^{-1}\rangle_{muca}/\langle W^{-1}\rangle_{muca}$. For recent reviews of these methodological aspects in the context of polymer simulations, see Refs. [76,77].

B. Observables

To obtain as much information as possible about the canonical equilibrium behavior, we define the following suitable quantities O. Next to the canonical expectation values $\langle O\rangle$, we also determine the fluctuations about these averages, as represented by the temperature derivative $d\langle O\rangle/dT = (\langle OE\rangle - \langle O\rangle\langle E\rangle)/T^2$. We use generic units, in which $k_B = 1$.

In order to identify conformational transitions, the specific heat (per monomer) $C_V(T) = (\langle E^2\rangle - \langle E\rangle^2)/NT^2$ with $\langle E^k\rangle = \sum_E g(E)E^k \exp(-E/T)/\sum_E g(E)\exp(-E/T)$ is calculated from the density of states $g(E)$. The density of states was found (up to an unimportant overall normalization constant) by reweighting the multicanonical energy distribution obtained with multicanonical sampling to the canonical distribution. Details are given in Ref. [66].

Apart from the specific heat, several structural quantities are of interest. In order to check the structural compactness of conformations or to identify the possible dispersion of conformations because of adsorption, the radius of gyration of the conformations is calculated. The radius of gyration is a measure for the extension of the polymer and defined by $R_g^2 \equiv \sum_{i=1}^N(\vec{r}_i - \vec{r}_{cm})^2/N = \sum_{i=1}^N\sum_{j=1}^N(\vec{r}_i - \vec{r}_j)^2/2N^2$ with $\vec{r}_{cm} = \sum_{i=1}^N \vec{r}_i/N$ being the center-of-mass location of the polymer.

We also calculated various shape descriptors derived from the gyration tensor [78–81] which is defined as

$$S = \frac{1}{N}\begin{pmatrix} \sum_i(x_i - x_{cm})^2 & \sum_i(x_i - x_{cm})(y_i - y_{cm}) & \sum_i(x_i - x_{cm})(z_i - z_{cm}) \\ \sum_i(x_i - x_{cm})(y_i - y_{cm}) & \sum_i(y_i - y_{cm})^2 & \sum_i(y_i - y_{cm})(z_i - z_{cm}) \\ \sum_i(x_i - x_{cm})(z_i - z_{cm}) & \sum_i(y_i - y_{cm})(z_i - z_{cm}) & \sum_i(z_i - z_{cm})^2 \end{pmatrix}. \quad (4)$$

Transformation to the principal axis system diagonalizes S,

$$S = \mathrm{diag}(\lambda_1, \lambda_2, \lambda_3), \quad (5)$$

where we assume that the eigenvalues of S are sorted in descending order, i.e., $\lambda_1 \geqslant \lambda_2 \geqslant \lambda_3$. The first invariant of S gives the squared radius of gyration,

$$\mathrm{Tr}\, S = \lambda_1 + \lambda_2 + \lambda_3 = R_g^2, \tag{6}$$

which agrees with the definition given above. The second invariant shape descriptor, or relative shape anisotropy, is defined as

$$\kappa^2 \equiv A_3 = \frac{3}{2}\frac{\mathrm{Tr}\hat{S}^2}{(\mathrm{Tr}S)^2} = 1 - 3\frac{\lambda_1\lambda_2 + \lambda_2\lambda_3 + \lambda_3\lambda_1}{(\lambda_1 + \lambda_2 + \lambda_3)^2}, \tag{7}$$

where $\hat{S} = S - \frac{1}{3}(\mathrm{Tr}S)I$ with unit tensor I. It reflects both the symmetry and dimensionality of a polymer conformation. This parameter is limited between the values of 0 and 1. It reaches 1 for an ideal linear chain and drops to zero for highly symmetric conformations. For planar symmetric objects, the relative shape anisotropy converges to the value of 1/4 [22,78–81].

The distance of the center of mass r_{cm} of the polymer to the surface also provides clear evidence that the polymer is freely moving or that it is very close to the surface and just adsorbed. Another useful quantity is the mean number of monomers $\langle N_s \rangle$ docked to the surface, which plays the role of an order parameter for the adsorption transition. A single-layer structure is formed if all monomers are attached at the sphere; if none is attached, the polymer is desorbed. The sphere potential is a continuous potential, and in order to distinguish monomers docked to the sphere from those not being docked, it is reasonable to introduce a cutoff. We define a monomer i as being "docked" if $r_i - R_s < r_c \equiv 1.2$. The corresponding measured quantity is the average number $\langle N_s \rangle$ of monomers docked to the surface. This can be expressed as $N_s = \sum_{i=1}^{N} \Theta(r_c - r_i)$, where $\Theta(r)$ is the Heaviside step function.

C. Computational details

In our simulations, the polymer chain length is $N = 20$ and we set $\epsilon = 1.0$ in the surface potential (2) large enough to allow adsorption of the polymer to the sphere surface. We consider two different situations: One is the case where the polymer is allowed to move freely in the space around the sphere over a distance $L = 60 - R_s$ from its surface (i.e., the nanosphere of radius R_s is centered in a spherical container of radius 60 with a purely steric wall), which is called the "free" or "nongrafted" case, and in the second case it is grafted with one end to the surface ("end grafted").

We have done simulations with different sizes of the sphere. The random initial configurations for the nongrafted and end-grafted cases of the simulation are sketched in Figs. 2(a) and 2(b). The total energy of the system is composed of the pure polymer chain energy $E_{\mathrm{LJ}} + E_{\mathrm{bend}}$ and the polymer chain attractive sphere interaction energy E_s. The initial configuration of the polymer chain is randomly generated. For the determination of the multicanonical weights we performed 200 iterations with at least 10^5 sweeps each. In the production period, 10^8 sweeps were generated to have reasonable statistics for estimating the thermodynamic quantities. Statistical errors are estimated with the standard jackknife technique [82–84].

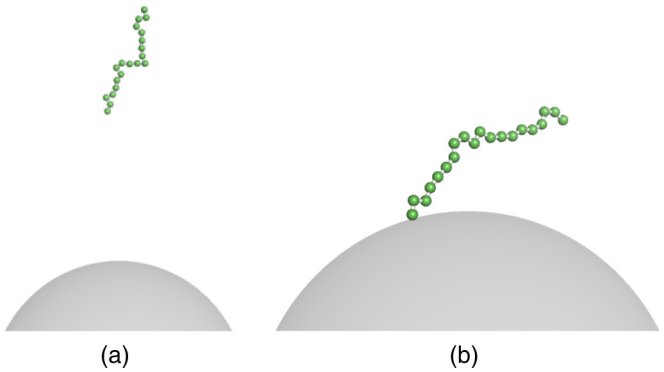

FIG. 2. Start configurations of the simulations: (a) non-grafted and (b) end-grafted polymers of length $N = 20$.

IV. RESULTS

A. Phase diagrams

To give an overview at the beginning, we start by presenting in Fig. 3 the main result of our study: The phase structure for (a) nongrafted and (b) end-grafted polymers derived from all of our observables as summarized by phase diagrams in the R_s-T plane. These phase diagrams are constructed by combining all the information coming from the canonical expectation values of our observables and their temperature derivatives described in more detail in the next two subsections. Some of our observables exhibit a peak at all of the transitions in the phase diagram, while others are only sensitive to one of them. For example, the collapse transition line at $T \approx 0.8$ is seen quite clearly from the peak in the temperature derivative of the canonical expectation value of the radius of gyration (6) and as a small shoulder in the invariant shape anisotropy (7). Naturally, this is further complemented by information coming directly from the eigenvalues of the gyration tensor. On the other hand, the adsorption transition line running roughly between $T \approx 1.5$ (small R_s) and $T \approx 2.5$ (large R_s) is most clearly constructed by looking at the mean distance of the center of mass of the polymer to the surface and the mean number of monomers adsorbed onto the surface, which plays the role of an order parameter for this transition. As discussed in more detail, for instance, in Ref. [20], since we are dealing with a finite system, it is not possible to determine the transition lines precisely: The transition lines still vary with chain length N and the observables have broad peaks. Thus we have a certain bandwidth which approximately covers the different peaks in the observables (and strictly speaking one should talk of "pseudotransitions" instead of "transitions" and "pseudophases" instead of "phases," but for brevity we will suppress the attribute "pseudo" in the following). Most of the transition lines in the phase diagrams (related to adsorption, collapse in three and two dimensions, freezing) approach strict phase transitions in the thermodynamic limit of infinitely long chains. Exceptions are the layering transitions at low temperatures whose locations are very sensitive to the finite chain length.

In the phase diagrams the radius of the sphere increases from left to right and the temperature increases from bottom to top. The grey bands separate the individual conformational phases. For high temperature, the polymer behaves in both

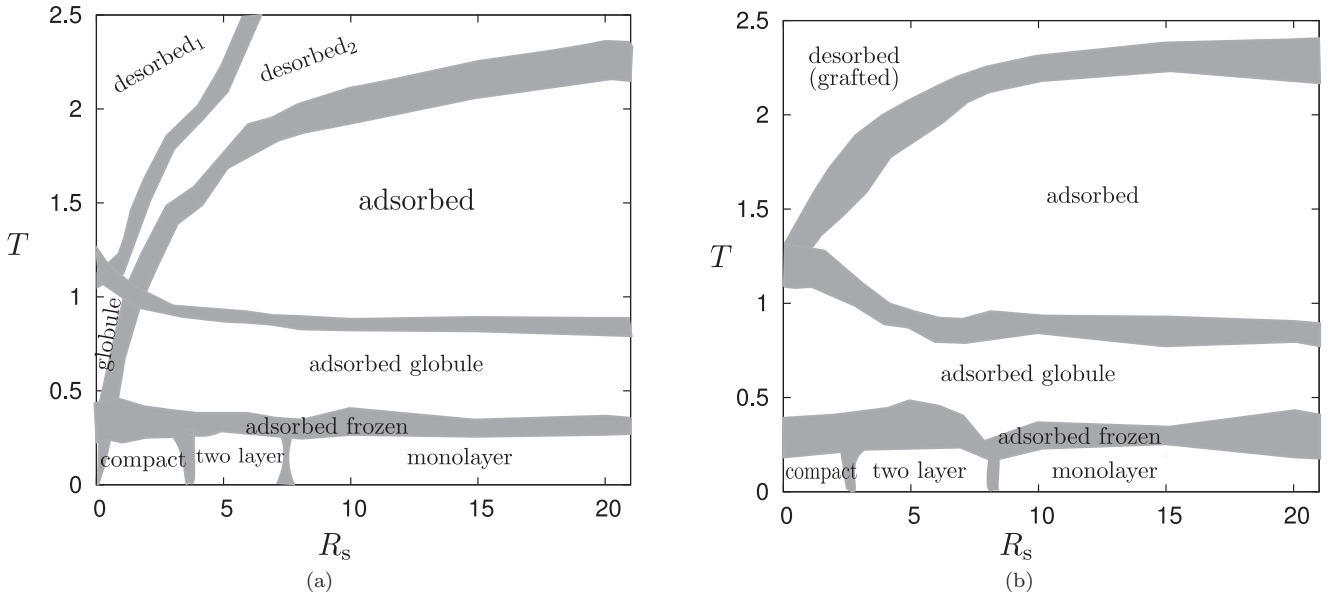

FIG. 3. The phase diagram of the homopolymer-attractive spherical surface system for (a) a nongrafted and (b) an end-grafted polymer as obtained from extensive multicanonical simulations. The grey bands separate the individual conformational phases. The bandwidth shows the variation of the peaks of temperature derivatives of different energetic and structural observables which have been analyzed simultaneously. In our simulations, the polymer chain length is $N = 20$ and we set $\epsilon = 1.0$ for the surface attraction strength.

cases similarly to a free polymer where the typical conformations are desorbed and extended random coils. In the nongrafted case with small sphere radius R_s, decreasing the temperature causes the (three-dimensional) collapse transition into globular conformations which are still in the desorbed phase. But below the freezing transition all the compact conformations are adsorbed. In contrast, for the end-grafted case all conformations are already adsorbed below the collapse transition. There is no desorbed globule phase in the grafted phase diagram. One more difference occurred also in the high-temperature desorbed phase. In the nongrafted case some structural observables give an indication for some changes in the desorbed phase. When we carefully analyze the conformations we see that those in the "desorbed$_1$" phase are far away from the sphere surface while the conformations in the "desorbed$_2$" phase are almost adsorbed. Thus they feel very strongly the surface effect. Because of the grafting, this is not the case for an end-grafted polymer. Increasing the sphere radius approximately to $R_s \approx 7.0$ leads to a very fast increase in the adsorption transition temperature, but after this value it increases slowly. The adsorption transition separates the regions of desorbed and adsorbed phases. Besides the collapse, adsorption, and freezing transitions, the most pronounced transition is the layering transition which occurs for low temperatures at $R_s \approx 7.0$ and separates the region of planar conformations which are monolayers of totally adsorbed conformations from the two-layer conformations. Another low-temperature transition is coming into play at $R_s \approx 3.0$, where two-layer conformations change to compact conformations (which look almost like a sphere).

The representative conformations that predominate in the different structural phases are depicted in Fig. 4 for the case of a nongrafted polymer. The observed structural phases for this case can be briefly summarized as follows:

Desorbed$_1$. Random coil structures with no surface contacts. These conformations freely circulate in the simulation space and are far away from the surface of the sphere [Fig. 4(a)].

Desorbed$_2$. Desorbed conformations, but they are almost adsorbed. The conformations feel the influence of the surface [Fig. 4(b)].

Adsorbed. Partially adsorbed, extended conformations [Fig. 4(c)].

Adsorbed globule. Partially adsorbed conformations [Fig. 4(d)].

Globule. Desorbed globule conformations. These conformations are only seen in the nongrafted phase diagram [Fig. 4(e)].

Compact. Partially adsorbed, globular conformations like a drop on the wall of the sphere [Fig. 4(f)].

Two layer. Partially adsorbed, compact conformations. These are two-layer structures. The lower layer of the conformations is adsorbed and lies on the wall of the sphere [Fig. 4(g)].

Monolayer. Completely adsorbed, compact conformations. These single-layer structures lie on the surface of the sphere and fit the sphere wall perfectly [Fig. 4(h)].

In the following two sections we will discuss in more detail how these phase diagrams have been obtained by analyzing energetic and structural observables.

B. Energetic fluctuations

Figure 5 displays the specific-heat curves $C_V(T)$ as a function of temperature T for different values of sphere radius R_s for (a) the nongrafted and (b) the end-grafted case. In both cases the specific heat signals two transitions: One is the low-temperature transition which is almost at the

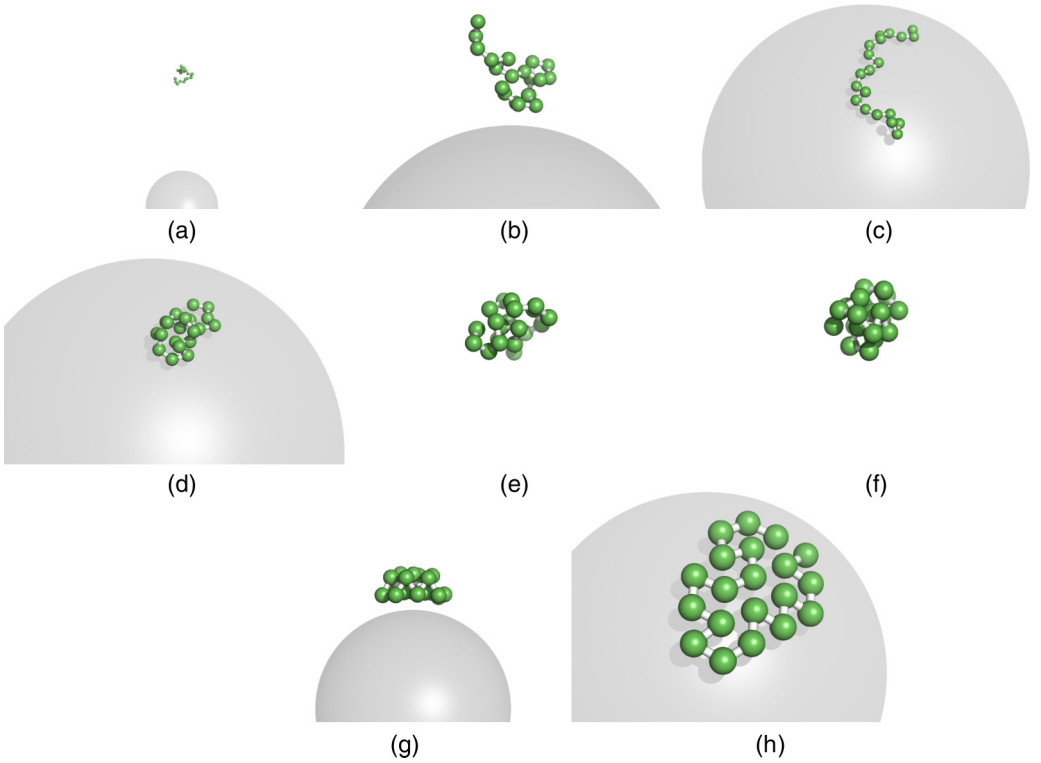

FIG. 4. Typical conformations for the regions (a) desorbed$_1$, (b) desorbed$_2$, (c) adsorbed, (d) adsorbed globule, (e) globule, (f) compact, (g) two layer, and (h) monolayer in the phase diagram for a nongrafted polymer.

same temperature ($T \approx 0.3$) for all different R_s values. This is the freezing transition which does not differ much for nongrafted and end-grafted chains. The second transition is quite pronounced in the nongrafted case but exhibits only a weak signal (a shoulder at $T \approx 2.0$) for the grafted polymer. This is the adsorption transition, which separates desorbed and adsorbed conformations. It comes into play at higher temperatures than the freezing transition and depends quite strongly on the sphere radius. This is consistent with previous observations that for nongrafted polymers of finite length this transition has a first-order-like signature (which eventually crosses over to second-order-like in the infinite chain-length limit) [8,21,52], whereas for grafted polymers it always looks like a continuous transition. In both cases, increasing the sphere radius causes an increase in the adsorption transition temperature.

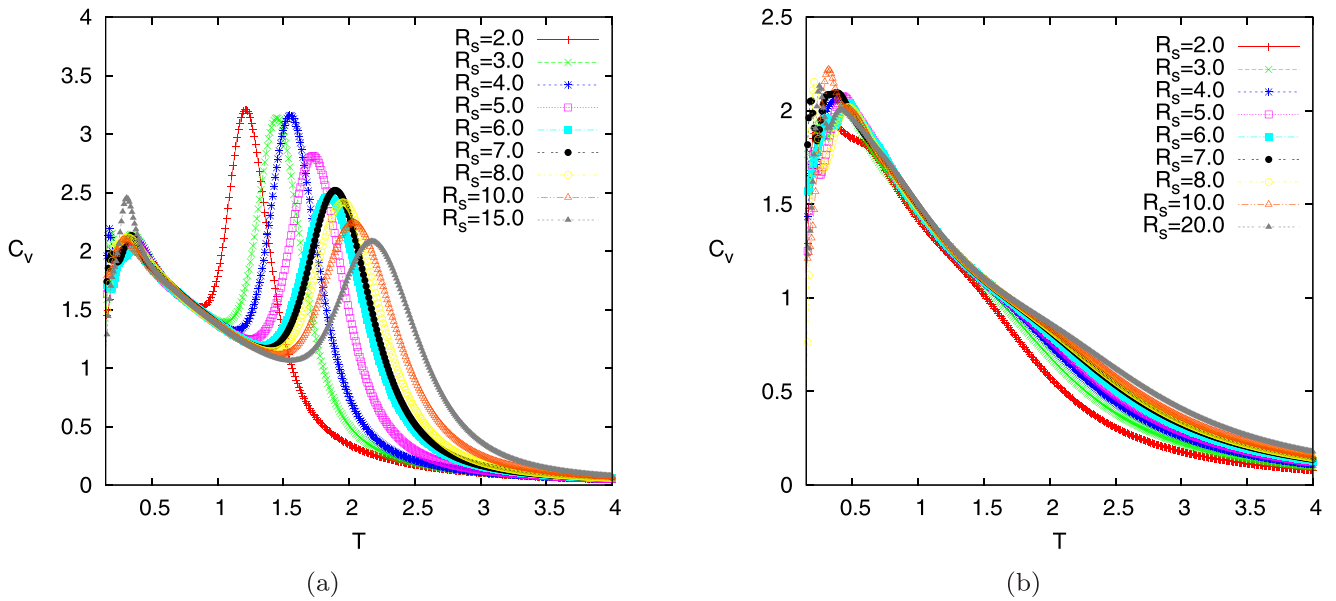

FIG. 5. Specific heat as a function of temperature for different sphere radii R_s for the (a) nongrafted and (b) end-grafted case (polymer length $N = 20$, surface attraction strength $\epsilon = 1.0$).

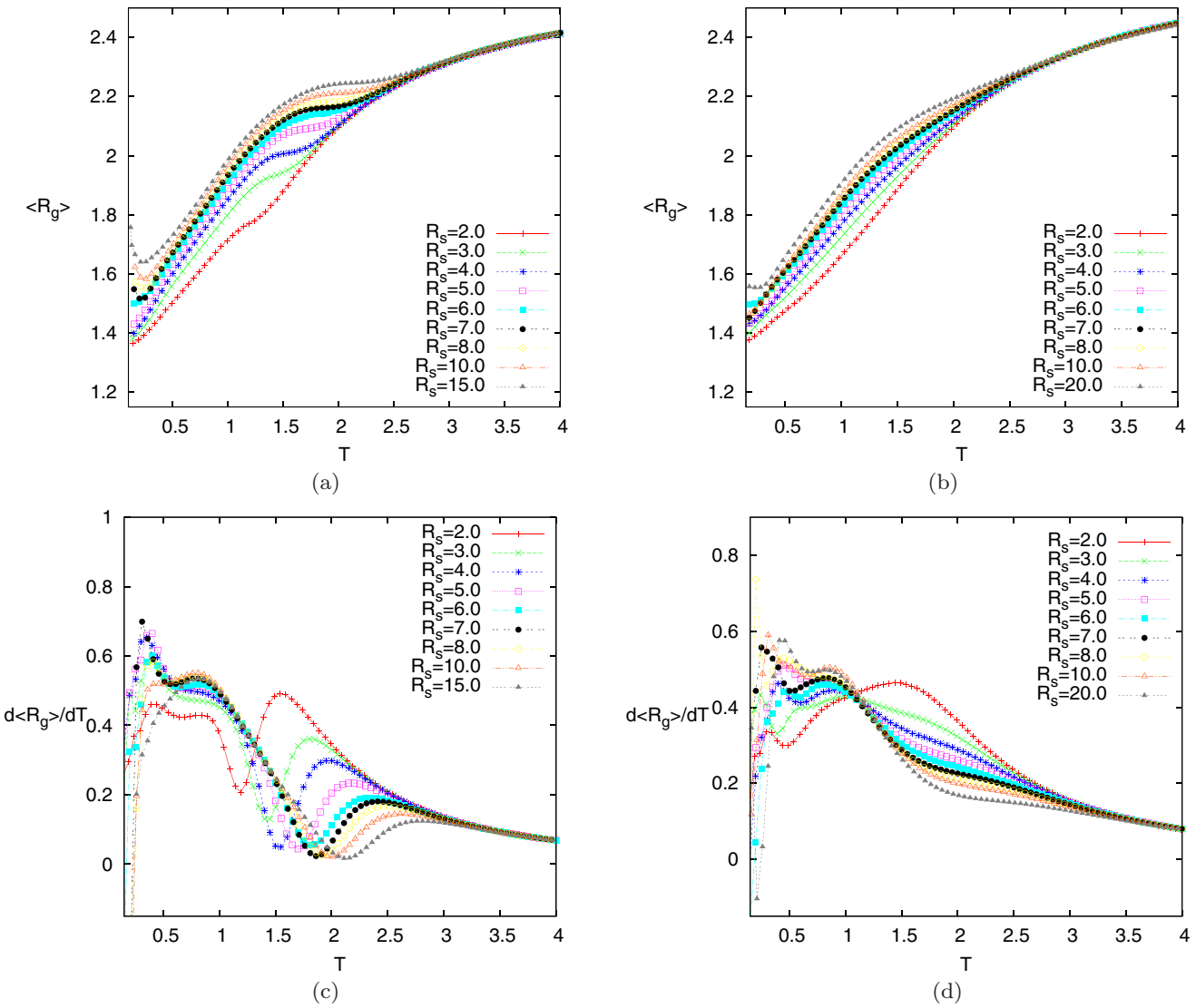

FIG. 6. The canonical expectation value of the radius of gyration $\langle R_g \rangle$ for the (a) nongrafted and (b) end-grafted case, and (c) and (d) the corresponding temperature derivatives, for different sphere radii R_s (polymer length $N = 20$, surface attraction strength $\epsilon = 1.0$).

C. Structural parameters and fluctuations

1. Radius of gyration R_g

The radius of gyration $\langle R_g \rangle$ (the first invariant of the gyration tensor) and its temperature derivative $d\langle R_g \rangle / dT$ are shown in Fig. 6 as a function of temperature for both the nongrafted and end-grafted cases, respectively. For small values of the sphere radius $R_s = 0.5, 1.0$, the most compact conformations occur in the low-temperature region with an average $\langle R_g \rangle \approx 1.23$ (data not shown). Slightly increasing the R_s value causes an increase in the average $\langle R_g \rangle$ value to about 1.4. Increasing the R_s parameter further, the curve for $R_s = 7.0$ of Fig. 6(a) in the nongrafted case has a minimum behavior at low temperatures. As a function of temperature the radius of gyration is monotonically increasing for all R_s values except beyond $R_s = 7.0$, where the layering transition occurs. Supporting information is also gained from the relative shape anisotropy parameter in Fig. 7. If we now look at the temperature derivative of the radius of gyration in Fig. 6(c), we detect three maxima for each R_s curve. The first peak at low temperatures ($T \approx 0.3$) indicates the freezing transition quite clearly, the second peak around $T \approx 0.8$ can be identified with the (two-dimensional) collapse transition, and the third, strongly moving peak in the region $T \approx 1.5$–3.0 signals the adsorption transition. For the end-grafted case these signals are generally weaker. In Fig. 6(d), the first two maxima are still discernible, but the adsorption transition is hardly reflected.

2. Invariant shape anisotropy parameter κ^2

Also the relative shape anisotropy parameter $\langle \kappa^2 \rangle$ (the second invariant of the gyration tensor) presented in Fig. 7 gives rich information and supports our findings derived from $\langle R_g \rangle$. As discussed above, in the nongrafted case, the desorbed phase is divided into two regions which are called "desorbed$_1$" and "desorbed$_2$." The boundary between these two regions is emerging in the temperature derivative $d\langle \kappa^2 \rangle / dT$ displayed in Fig. 7(c) (and also in $d\langle R_g \rangle / dT$) as a second peak at high temperatures, since the peaks are going to become invisible with increasing R_s values and also are smaller than the peaks at low temperatures. We have investigated the conformations

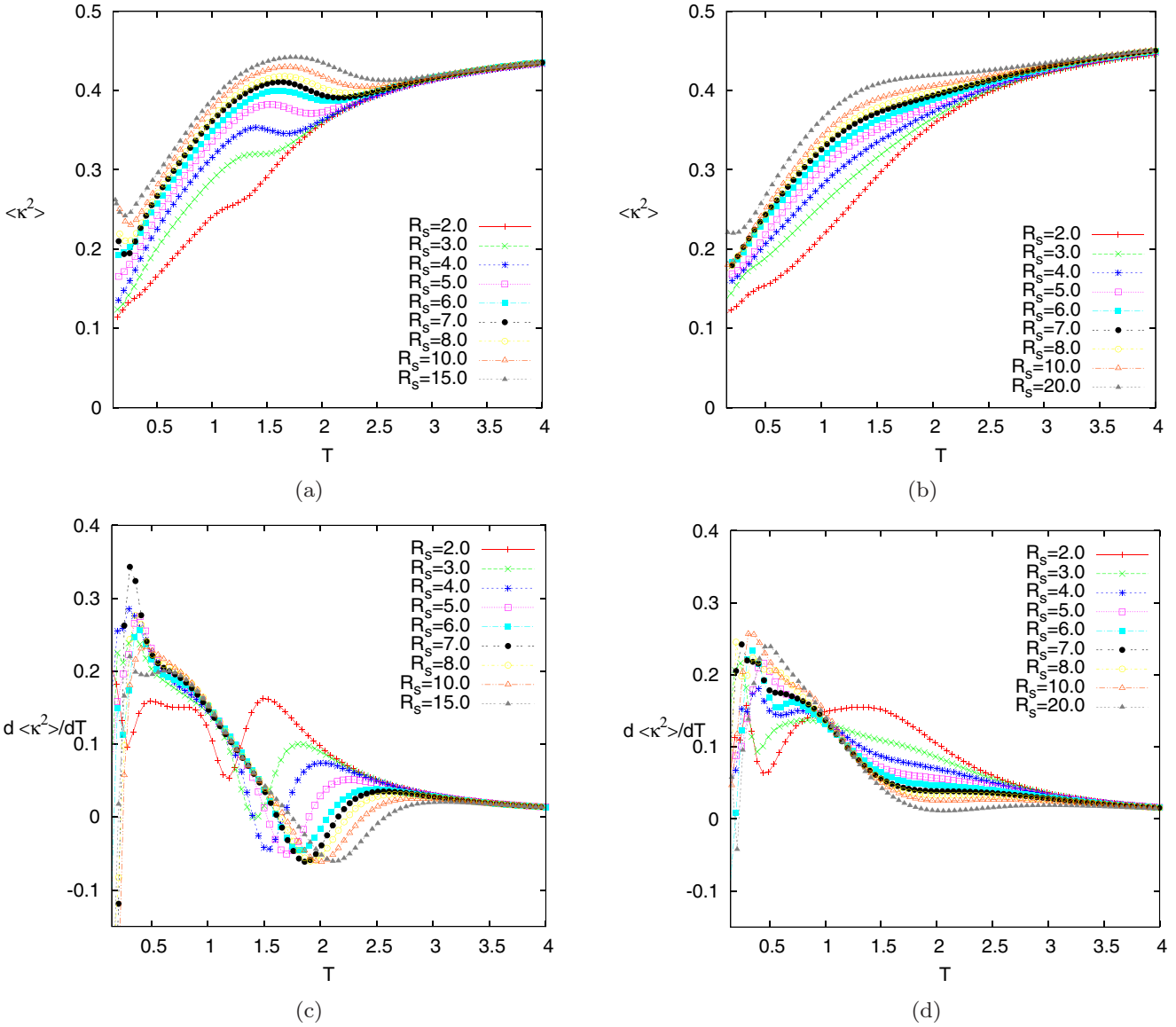

FIG. 7. The canonical expectation value of the relative shape anisotropy parameter $\langle\kappa^2\rangle$ for the (a) nongrafted and (b) end-grafted case, and (c) and (d) the corresponding temperature derivatives, for different sphere radii R_s (polymer length $N = 20$, surface attraction strength $\epsilon = 1.0$).

in both regions in detail and concluded that the conformations in the desorbed$_1$ phase are far away from the surface. On the other hand, the conformations in the desorbed$_2$ phase are almost adsorbed to the sphere boundary, which indicates the influence of the surface on the desorbed phase. Additionally, the relative shape anisotropy parameter $\langle\kappa^2\rangle$ clearly gives the phase boundaries at very low temperatures (below the freezing transition at $T \approx 0.3$). The curves in Fig. 7(a) belonging to different R_s values are grouped at very low temperatures into different κ^2 values, indicating the boundaries from compact to two-layer phase, and from two-layer to monolayer phase in the phase diagrams.

3. *Center-of-mass distance r_{cm} and number of adsorbed monomers N_s*

The adsorption transition can be best detected by the distance of the center of mass of the polymer to the substrate $r_{cm} - R_s$ and by the number of adsorbed monomers N_s, where a monomer is defined to be adsorbed onto the surface if $r_i - R_s < 1.2$. The behavior of these two observables, in particular the peaks in their temperature derivative, build the adsorption line in the phase diagrams. Figures 8(a) and 8(b) give the distance of the center of mass of the polymer to the sphere surface for the nongrafted and end-grafted cases, respectively. As can be seen in Fig. 8(a), for high temperatures the nongrafted polymer can move freely within the simulation space and the influence of the surface is minimal for large R_s values, whereas for small R_s the influence is mainly steric. Thus, the average center-of-mass distance of the polymer above the surface is nearly half of the simulation space. In contrast, at low temperatures the polymer favors surface contacts and the average center-of-mass distance converges to the minimum location of the potential (cf. Fig. 1). One can clearly detect a quite pronounced peak in its temperature

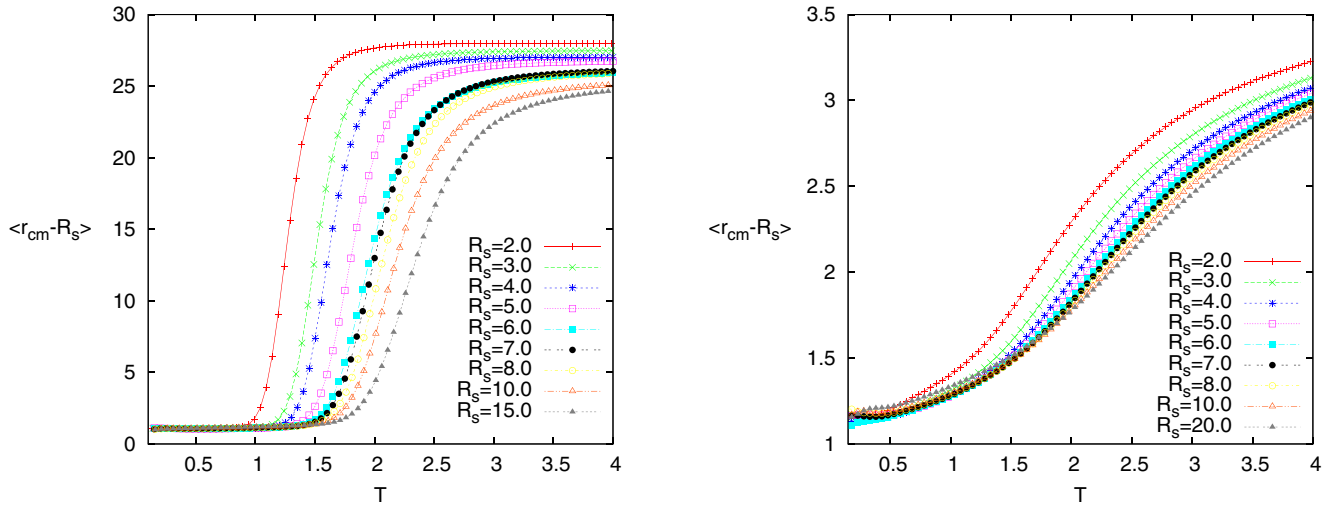

FIG. 8. The canonical expectation value of the distance of the center of mass of the polymer $\langle r_{\rm cm}\rangle$ from the sphere surface for the (a) nongrafted and (b) end-grafted case (polymer length $N = 20$, surface attraction strength $\epsilon = 1.0$).

derivative (see the Appendix) that divides the phase space into adsorbed and desorbed phases. Consistently with our discussion above, the pronounced tendency of the polymer to make surface contacts can also be identified from the mean number of adsorbed monomers to the surface $\langle N_{\rm s}\rangle$ shown in Fig. 9 and the (negative) minima in its temperature derivative (see the Appendix). They are in good agreement with the sharp peaks in the temperature derivative of the distance of the center of mass of the polymer which together draw the adsorption line in the phase diagram. By comparing the end-grafted with the nongrafted case, the main difference is found at the adsorption transition: A crossover occurs from low temperature, where the polymer is adsorbed and the conformations of an end-grafted and a nongrafted polymer are very similar, to high temperatures, where the nongrafted polymer approaches the behavior of a polymer in bulk solution while that of an end-grafted polymer is always affected by the attractive sphere surface. Because of this effect, the adsorption transition for the end-grafted chain is much smoother which can be clearly seen in the $\langle r_{\rm cm}\rangle$ and $\langle N_s\rangle$ parameters in Figs. 8(b) and 9(b). In contrast, the adsorption of a nongrafted chain exhibits a first-order-like signature which is also clear from the same structural parameters. Because in the nongrafted case these quantities change sharply as soon as the polymer desorbs, it leaves the influence of the surface field. An end-grafted polymer, on the other hand, cannot leave the surface field.

4. Eigenvalues of the gyration tensor

Finally, the eigenvalues of the gyration tensor which measure the extensions in the principle axis system are extracted to complement the picture. In Figs. 10(a)–10(c) they are displayed for different values of $R_{\rm s}$ for the nongrafted

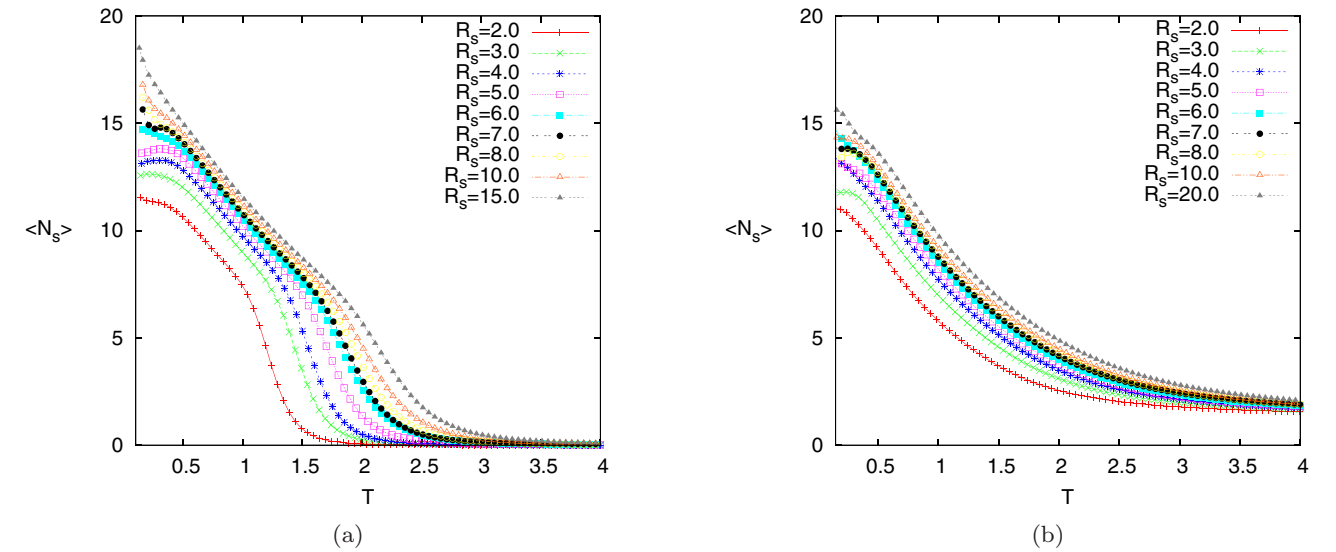

FIG. 9. The canonical expectation value of the mean number of docked monomers $\langle N_{\rm s}\rangle$ for the (a) nongrafted and (b) end-grafted case (polymer length $N = 20$, surface attraction strength $\epsilon = 1.0$).

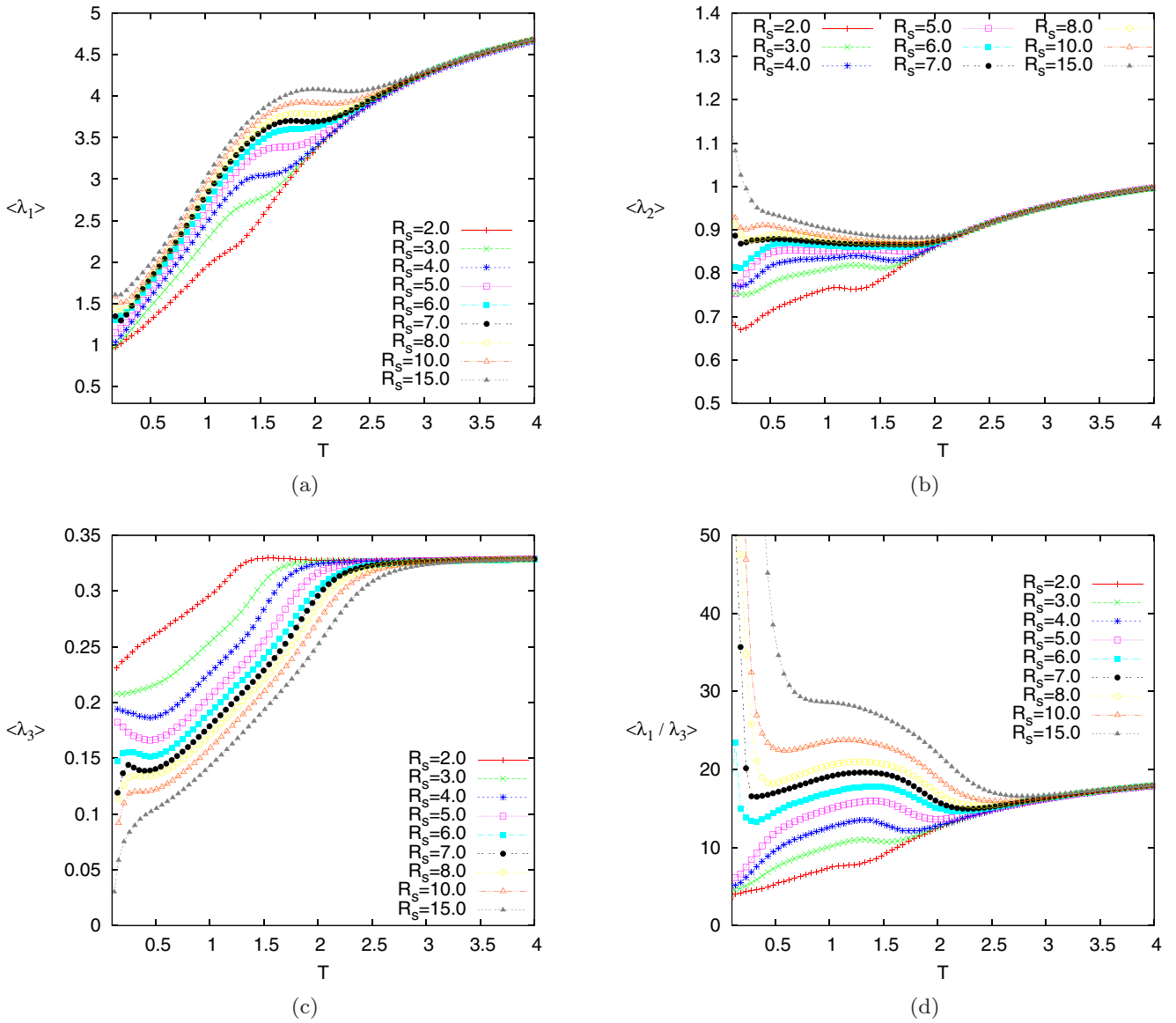

FIG. 10. The canonical expectation values of the three eigenvalues $\langle\lambda_1\rangle$, $\langle\lambda_2\rangle$, and $\langle\lambda_3\rangle$ of the gyration tensor and the ratio of the largest to the smallest eigenvalue $\langle\lambda_1/\lambda_3\rangle$ for a nongrafted polymer in the presence of an attractive sphere with different radii R_s (polymer length $N = 20$, surface attraction strength $\epsilon = 1.0$).

case. For high temperatures they are in good agreement with the results in our previous study [55], showing the same limit values of the three eigenvalues for random-coil structures, and overall they all support our earlier findings described above. For low temperatures, the curves in Figs. 10(a)–10(c) belonging to different R_s values are also grouped into different $\langle\lambda_1\rangle$, $\langle\lambda_2\rangle$, and $\langle\lambda_3\rangle$ values, indicating the boundaries (grey bands) in the phase diagrams which are detected from the other structural quantities. The most important result deducible from the eigenvalues is that the third eigenvalue of the gyration tensor $\langle\lambda_3\rangle$ converges to small values which means that the extension in the third direction vanishes and the conformations are two-dimensional objects signaling the layering transition. To highlight this finding we show in Fig. 10(d) the ratio of the largest to the smallest eigenvalue $\langle\lambda_1/\lambda_3\rangle$. For low temperatures below $T \approx 0.3$, this ratio assumes relatively small values until $R_s \approx 6.0$. Above $R_s \approx 7.0$ the ratio of the eigenvalues jumps to very much larger values, confirming that the layering transition occurs at this R_s value, which separates the conformational space from planar conformations. This signal is also reflected in the corresponding temperature derivatives which are compiled in the Appendix.

V. CONCLUSION

In this paper, we have reported results from extensive multicanonical Monte Carlo computer simulations for investigating the full conformational behavior of a generic coarse-grained finite polymer chain near an attractive spherical surface. In a systematic analysis, over a wide range of sphere radius R_s and temperature T, we have constructed the entire phase diagrams for both nongrafted and end-grafted polymers. For the identification of the conformational phases, we have examined several energetic and structural observables and their

fluctuations by canonical statistical analysis. The transition lines in the phase diagrams show the best match of all observables analyzed simultaneously in our study. In the thermodynamic limit of infinitely long chains the transitions are expected to occur at sharp values of the parameters. For finite chains, on the other hand, the transition lines still vary with chain length N and are not well defined because of broad peaks in the observables that also have small differences in between. Therefore the locations of the phase boundaries should be considered as a rough guide. However, even for the rather short chains considered here, we can clearly identify different phases which show distinguishing features, so that a reasonable picture is obtained. Most of the phases are believed to still persist for longer chains. An exception are the layered phases which depend very sensitively on the finite chain length. All our results obtained from the different observables are summarized in the phase diagrams in the R_s-T plane which for a convenient overview are displayed at the beginning of the results section in Fig. 3(a) for nongrafted and in Fig. 3(b) for end-grafted polymers, respectively.

It is clear that, for longer chains, the desorbed, globule, and compact phases will survive. Additionally, filmlike (monolayer) and semispherical conformations (two layer) as well as surface attached globular shapes will dominate the respective phases. On the other hand, as long as surface effects are as influential as volume effects the compact adsorbed conformations differ noticeably for polymers with different but small lengths. But, for the majority of phases we find qualitative coincidence with a simple coarse-grained model.

In this study, we kept the adsorption field constant (whereas we varied the adsorption strength in another earlier study) and varied the radius of the nanoparticles and observed qualitatively the described scenarios. As a result, our model system can be mapped in the considered parameter range to real systems considered in experiments. For example, based on early experimental results [85,86], Feng and Ruckenstein [45] examined the adsorption of a specific polyampholyte chain on a single spherical nanoparticle with three different radii. In this application, the charge density at the particle surface regulates the strength of the adsorption field (corresponding to our parameter ϵ) and the polymer composition regulates the location of the coil-globule transition (corresponding to ϵ_{LJ}). Compared with experimental findings, computational studies of generic coarse-grained models have the advantage that different combinations of parameters can be varied over wide ranges. In this way, a specific detailed system can be put into a broader context and a deeper understanding based on fundamental principles of statistical physics can be gained.

ACKNOWLEDGMENTS

We wish to thank V. Blavatska and B. Abel for useful discussions. H.A. acknowledges support by the Alexander von Humboldt Foundation (AvH) under the Experienced Researcher Fellowship Programme. W.J. thanks the Deutsche Forschungsgemeinschaft (DFG) for support through the Collaborative Research Centre SFB/TRR 102 (Project No. B04) and under Grant No. JA 483/33-1. We also benefited from the Marie Curie IRSES network DIONICOS under Contract No. PIRSES-GA-2013-612707 within the European Union Seventh Framework Programme. The computer time for the Monte Carlo simulations was provided by NIC, Forschungszentrum Jülich, under Grant No. hlz24, which we gratefully acknowledge.

APPENDIX

Next to the expectation values $\langle O\rangle$ of all structural quantities discussed in our main text, we also determined the fluctuations of these structural quantities, as represented by the temperature derivative $d\langle O\rangle/dT = (\langle OE\rangle - \langle O\rangle\langle E\rangle)/T^2$. We use generic units, in which $k_B = 1$. The fluctuations of all structural quantities not discussed in the main text are shown in Figs. 11–13.

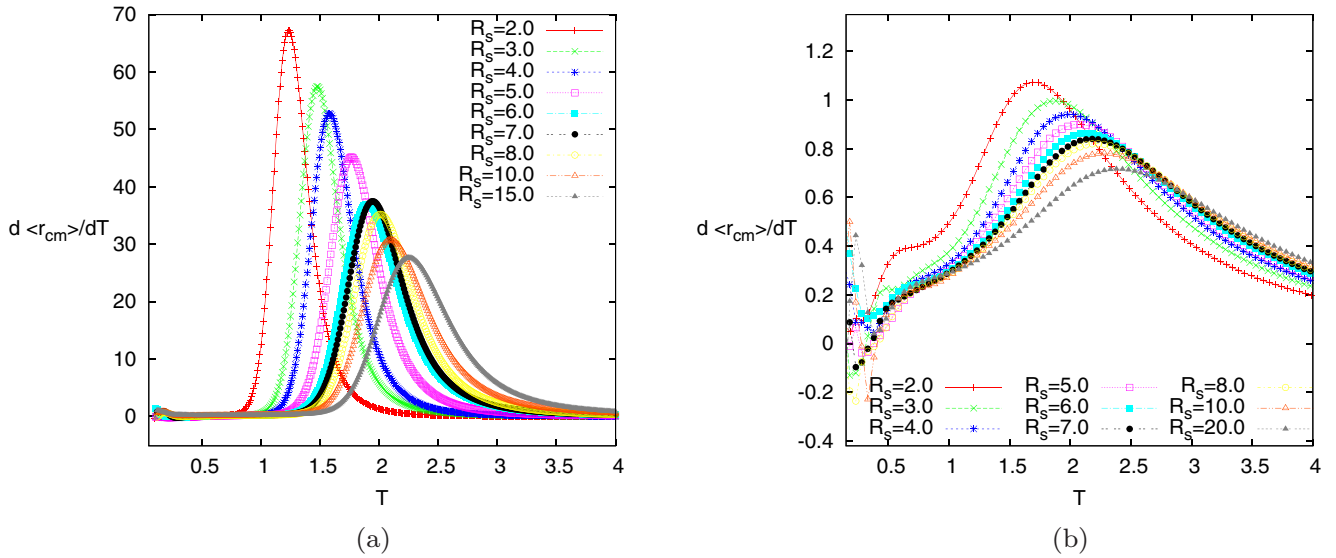

FIG. 11. The fluctuations of the distance of the center of mass of the polymer from the sphere surface for (a) the nongrafted and (b) the end-grafted case.

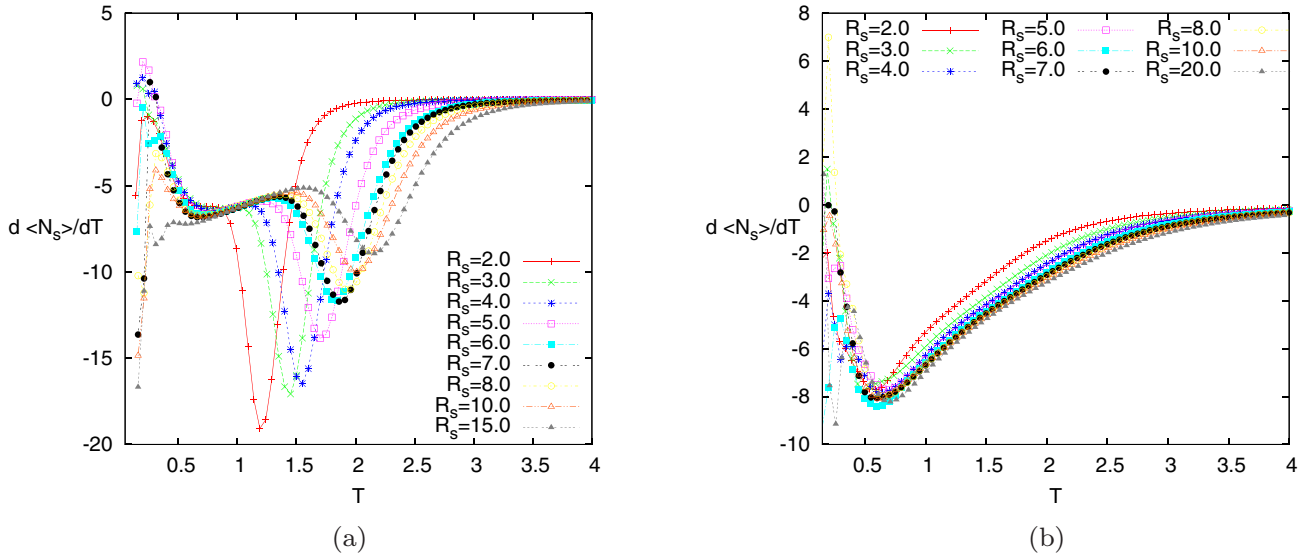

FIG. 12. The fluctuations of the number of adsorbed monomers for (a) the nongrafted and (b) the end-grafted case.

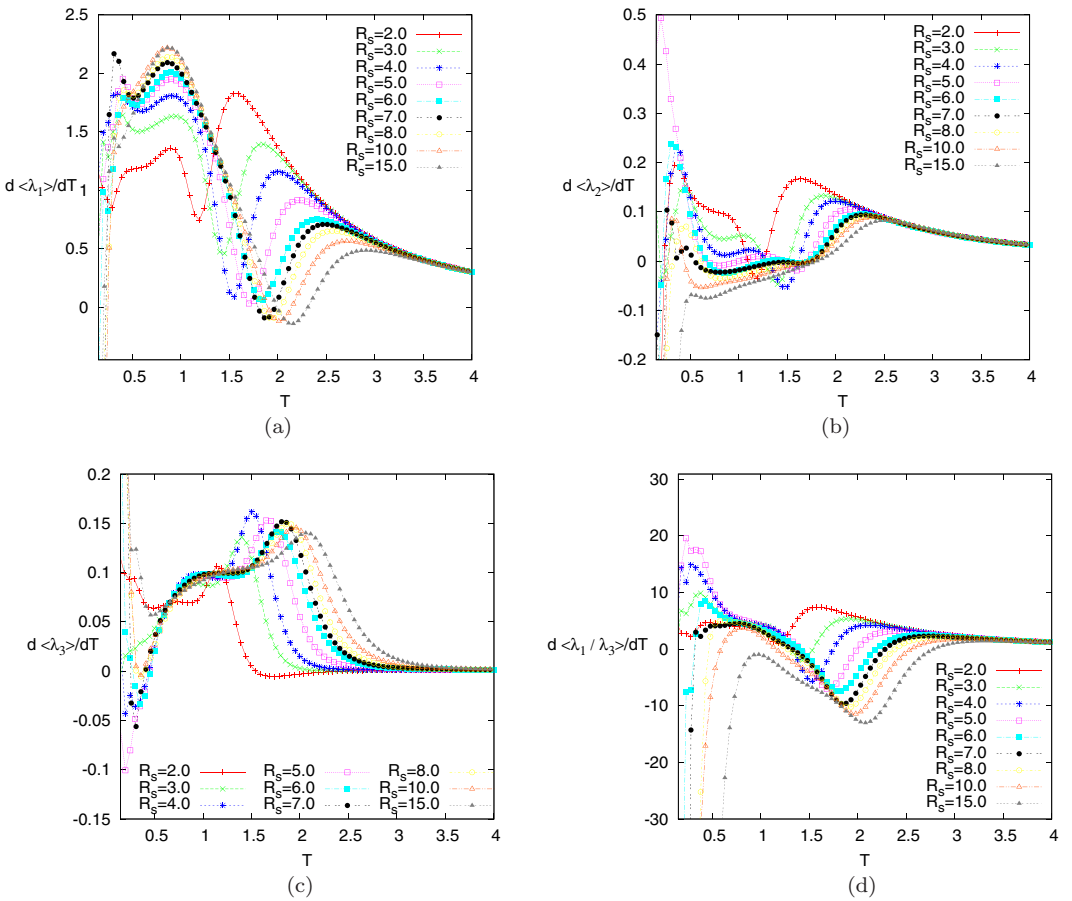

FIG. 13. The fluctuations of the three eigenvalues (a) $\langle\lambda_1\rangle$, (b) $\langle\lambda_2\rangle$, (c) $\langle\lambda_3\rangle$ of the gyration tensor and (d) the fluctuations of the ratio of the largest eigenvalue to the smallest eigenvalue $\langle\lambda_1/\lambda_3\rangle$ for different sphere radii R_s for the nongrafted case.

[1] R. F. Service, Science **270**, 230 (1995).
[2] S. Walheim, E. Schaffer, J. Mlynek, and U. Steiner, Science **283**, 520 (1999).
[3] S. Brown, Nat. Biotechnol. **15**, 269 (1997).
[4] R. Braun, M. Sarikaya, and K. Schulten, J. Biomater. Sci., Polym. Ed. **13**, 747 (2002).
[5] S. R. Whaley, D. S. English, E. L. Hu, P. F. Barbara, and A. M. Belcher, Nature (London) **405**, 665 (2000).
[6] K. Goede, P. Busch, and M. Grundmann, Nano Lett. **4**, 2115 (2004).
[7] M. Bachmann, K. Goede, A. G. Beck-Sickinger, M. Grundmann, A. Irbäck, and W. Janke, Angew. Chem. Int. Ed. **49**, 9530 (2010).
[8] E. Eisenriegler, K. Kremer, and K. Binder, J. Chem. Phys. **77**, 6296 (1982).
[9] R. Descas, J.-U. Sommer, and A. Blumen, J. Chem. Phys. **120**, 8831 (2004).
[10] M. Bachmann and W. Janke, Phys. Rev. Lett. **95**, 058102 (2005).
[11] M. Bachmann and W. Janke, Phys. Rev. E **73**, 020901(R) (2006).
[12] M. Bachmann and W. Janke, Phys. Rev. E **73**, 041802 (2006).
[13] J. Luettmer-Strathmann, F. Rampf, W. Paul, and K. Binder, J. Chem. Phys. **128**, 064903 (2008).
[14] M. Bachmann and W. Janke, in *Rugged Free Energy Landscapes: Common Computational Approaches to Spin Glasses, Structural Glasses and Biological Macromolecules*, edited by W. Janke, Lecture Notes in Physics No. 736 (Springer, Berlin, 2008), pp. 203–246.
[15] M. Möddel, M. Bachmann, and W. Janke, J. Phys. Chem. B **113**, 3314 (2009).
[16] V. A. Ivanov, J. A. Martemyanova, M. Müller, W. Paul, and K. Binder, J. Phys. Chem. B **113**, 3653 (2009).
[17] T. Chen, L. Wang, X. Lin, Y. Liu, and H. Liang, J. Chem. Phys. **130**, 244905 (2009).
[18] L. Wang, T. Chen, X. Lin, Y. Liu, and H. Liang, J. Chem. Phys. **131**, 244902 (2009).
[19] A. D. Swetnam and M. P. Allen, Phys. Chem. Chem. Phys. **11**, 2046 (2009).
[20] M. Möddel, W. Janke, and M. Bachmann, Phys. Chem. Chem. Phys. **12**, 11548 (2010).
[21] M. Möddel, W. Janke, and M. Bachmann, Macromolecules **44**, 9013 (2011).
[22] V. Blavatska and W. Janke, J. Chem. Phys. **136**, 104907 (2012).
[23] Y. W. Li, T. Wüst, and D. P. Landau, Phys. Rev. E **87**, 012706 (2013).
[24] M. Möddel, W. Janke, and M. Bachmann, Phys. Rev. Lett. **112**, 148303 (2014).
[25] M. P. Taylor and J. Luettmer-Strathmann, J. Chem. Phys. **141**, 204906 (2014).
[26] K. S. Austin, J. Zierenberg, and W. Janke, Macromolecules **50**, 4054 (2017).
[27] J. Krawczyk, A. L. Owczarek, T. Prellberg, and A. Rechnitzer, J. Stat. Mech.: Theory Exp. (2005) P05008.
[28] S. Bhattacharya, V. G. Rostiashvili, A. Milchev, and T. A. Vilgis, Phys. Rev. E **79**, 030802(R) (2009).
[29] M. J. Russell, Science **302**, 580 (2003).
[30] M. Lundqvist, P. Nygren, B.-H. Jonsson, and K. Broo, Angew. Chem. Int. Ed. **45**, 8169 (2006).
[31] I. Gurevitch and S. Srebnik, Chem. Phys. Lett. **444**, 96 (2007).
[32] I. Gurevitch and S. Srebnik, J. Chem. Phys. **128**, 144901 (2008).
[33] T. Vogel and M. Bachmann, Phys. Rev. Lett. **104**, 198302 (2010).
[34] T. Vogel, J. Gross, and M. Bachmann, J. Chem. Phys. **142**, 104901 (2015).
[35] M. Tagliazucchi, M. Olvera de la Cruz, and I. Szleifer, Proc. Natl. Acad. Sci. USA **107**, 5300 (2010).
[36] K. I. Skau and E. M. Blokhuis, Macromolecules **36**, 463 (2003).
[37] R. R. Netz and J.-F. Joanny, Macromolecules **31**, 5123 (1998).
[38] S. A. Barr and A. Z. Panagiotopoulos, J. Chem. Phys. **137**, 144704 (2012).
[39] A. Gladytz, M. Wagner, T. Häupl, C. Elsner, and B. Abel, Part. Part. Syst. Char. **32**, 573 (2015).
[40] C. Elsner, D. Hintzen, A. Prager, K. R. Siefermann, and B. Abel, Z. Phys. Chem. **229**, 427 (2015).
[41] A. Gladytz, B. Abel, and H. J. Risselada, Angew. Chem. Int. Ed. **55**, 11242 (2016).
[42] T. A. Kampmann, H.-H. Boltz, and J. Kierfeld, J. Chem. Phys. **139**, 034903 (2013).
[43] M. Tanaka, A. Yu. Grosberg, and T. Tanaka, J. Chem. Phys. **110**, 8176 (1999).
[44] M. Tanaka and T. Tanaka, Phys. Rev. E **62**, 3803 (2000).
[45] J. Feng and E. Ruckenstein, Polymer **44**, 3141 (2003).
[46] J. McNamara, C. Y. Kong, and M. Muthukumar, J. Chem. Phys. **117**, 5354 (2002).
[47] J. Wang and M. Muthukumar, J. Chem. Phys. **135**, 194901 (2011).
[48] R. Messina, Macromolecules **37**, 621 (2004).
[49] A. V. Dobrynin and M. Rubinstein, Prog. Polym. Sci. **30**, 1049 (2005).
[50] A. V. Dobrynin, Curr. Opin. Colloid Interface Sci. **13**, 376 (2008).
[51] R. R. Netz and J.-F. Joanny, Macromolecules **32**, 9013 (1999).
[52] R. R. Netz and D. Andelman, Phys. Rep. **380**, 1 (2003).
[53] M. Marenz, J. Zierenberg, H. Arkın, and W. Janke, Condens. Matter Phys. **15**, 43008 (2012).
[54] H. Arkın and W. Janke, Phys. Rev. E **85**, 051802 (2012).
[55] H. Arkın and W. Janke, J. Chem. Phys. **138**, 054904 (2013).
[56] H. Arkın and W. Janke, J. Phys. Chem. B **116**, 10379 (2012).
[57] H. Arkın and W. Janke, Eur. Phys. J.: Spec. Top. **216**, 181 (2013).
[58] T. Bogner, A. Degenhard, and F. Schmid, Phys. Rev. Lett. **93**, 268108 (2004).
[59] E. Balog, T. Becker, M. Oettl, R. Lechner, R. Daniel, J. Finney, and J. C. Smith, Phys. Rev. Lett. **93**, 028103 (2004).
[60] M. Ikeguchi, J. Ueno, M. Sato, and A. Kidera, Phys. Rev. Lett. **94**, 078102 (2005).
[61] N. Gupta and A. Irbäck, J. Chem. Phys. **120**, 3983 (2004).
[62] F. H. Stillinger, T. Head-Gordon, and C. L. Hirshfeld, Phys. Rev. E **48**, 1469 (1993).
[63] F. H. Stillinger and T. Head-Gordon, Phys. Rev. E **52**, 2872 (1995).
[64] A. Irbäck, C. Peterson, F. Potthast, and O. Sommelius, J. Chem. Phys. **107**, 273 (1997).
[65] A. Irbäck, C. Peterson, and F. Potthast, Phys. Rev. E **55**, 860 (1997).
[66] M. Bachmann, H. Arkın, and W. Janke, Phys. Rev. E **71**, 031906 (2005).
[67] M. Marenz and W. Janke, Phys. Rev. Lett. **116**, 128301 (2016).

[68] S. J. Marrink, H. J. Risselada, S. Yefimov, D. P. Tieleman, and A. H. de Vries, J. Phys. Chem. B **111**, 7812 (2007).
[69] A. L. Rodriguez, C. Vega, and J. J. Freire, J. Chem. Phys. **111**, 438 (1999).
[70] B. A. Berg and T. Neuhaus, Phys. Lett. B **267**, 249 (1991).
[71] B. A. Berg and T. Neuhaus, Phys. Rev. Lett. **68**, 9 (1992).
[72] W. Janke, Int. J. Mod. Phys. C **3**, 1137 (1992).
[73] B. A. Berg, in *Monte Carlo Methods*, edited by N. Madras, Fields Institute Communications (American Mathematical Soc., Providence, Rhode Island, 2000), Vol. 26, pp. 1–24.
[74] W. Janke, Physica A **254**, 164 (1998).
[75] W. Janke, in *Computer Simulations of Surfaces and Interfaces*, NATO Science Series II, Vol. 114, edited by B. Dünweg, D. P. Landau, and A. I. Milchev (Kluwer, Dordrecht, 2003), pp. 137–157.
[76] W. Janke and W. Paul, Soft Matter **12**, 642 (2016).
[77] J. Zierenberg, M. Marenz, and W. Janke, Polymers **8**, 333 (2016).
[78] K. Solc and W. H. Stockmayer, J. Chem. Phys. **54**, 2756 (1971).
[79] D. N. Theodorou and U. W. Suter, Macromolecules **18**, 1206 (1985).
[80] V. Blavatska and W. Janke, J. Chem. Phys. **133**, 184903 (2010).
[81] J. Vymětal and J. Vondrášek, J. Phys. Chem. A **115**, 11455 (2011).
[82] B. Efron, *The Jackknife, the Bootstrap and Other Resampling Plans* (Society for Industrial and Applied Mathematics, Philadelphia, 1982).
[83] W. Janke, in *Computational Many-Particle Physics*, Wilhelm & Else Heraeus Summerschool, Greifswald, edited by H. Fehske, R. Schneider, and A. Weiße, Lecture Notes in Physics No. 739 (Springer, Berlin, 2008), pp. 79–140.
[84] W. Janke, in *Order, Disorder and Criticality: Advanced Problems of Phase Transition Theory*, edited by Y. Holovatch (World Scientific, Singapore, 2012), Vol. 3, pp. 93–166.
[85] V. Lesins and E. Ruckenstein, Colloid Polym. Sci. **266**, 1187 (1988).
[86] V. Lesins and E. Ruckenstein, J. Colloid Interface Sci. **132**, 566 (1989).